第 44 卷 第 3 期/2024 年 2 月/光学学报 研究论文

光学学报

基于双频泵浦正常色散富硅氮化硅微环谐振腔的光频率梳设计

杨亚楠[1]，高荣[1]，湛晨翌[1]，李丁[1]，邓宜[1]，王子潇[1]，梁坤[2]，冯素春[1*]

[1]北京交通大学电子信息工程学院光波技术研究所全光网络与现代通信网教育部重点实验室，北京 100044；

[2]北京交通大学电子信息工程学院，北京 100044

摘要 提出一种利用锁相双频激光作为泵浦源输入正常色散富硅氮化硅微环谐振腔产生光频率梳的方案。对富硅氮化硅微环谐振腔进行色散调控，实现1550 nm波段平坦正常色散优化设计。利用LLE（Lugiato Lefever equation）方程进行光频率梳产生仿真，分析改变泵浦失谐时光频率梳产生的时域和频域演化过程。同时，探究各项参数对光频率梳产生的影响，包括泵浦功率、双频激光功率占比、微腔波导损耗、微腔色散、双频激光频率间隔。仿真实现的光频率梳带宽可覆盖1520 nm到1580 nm。

关键词 非线性光学；光频率梳；富硅氮化硅；色散调控；微腔

中图分类号 TN252 **文献标志码** A **DOI** 10.3788/AOS231593

1 引 言

光频率梳是一种具有固定重复频率的超短光脉冲，频域具有等频率间隔，可以将光学频率相干地连接到微波频率，目前已经广泛应用于气体检测、天文光谱、光学频率计量和高速大容量光通信等领域。本文重点关注在光通信和微波光子领域有着较大应用需求的频率间隔在10～200 GHz的光频率梳，这类光频率梳的应用不要求实现自参考（self reference）。目前，产生光频率梳的方法主要有4种：1）基于锁模激光器[1-3]，该方法获得的光频率梳频率间隔不易调谐；2）基于电光调制[4]，该方法通过级联电光调制器实现光频率梳，中心频率和频率间隔均可实现调谐，但产生的光频率梳梳齿个数较少；3）基于非线性超连续谱展宽[5]，该方法将较高峰值功率的光脉冲输入非线性介质，利用色散和非线性相互作用实现超连续谱展宽；4）基于克尔（Kerr）微环谐振腔[6-8]，该方法将单频激光输入Kerr微环谐振腔中，使光场在微腔中不断循环积累，利用色散和四波混频等非线性效应的共同作用产生光频率梳，易于实现小型化。

基于Kerr微环谐振腔的集成光频率梳受到研究人员广泛关注。目前，反常色散区光频率梳存在诸如泵浦转换效率不高、长期稳定性不好等问题，严重制约了微腔光频率梳的实际应用。在正常色散区实现的光频率梳具有泵浦转换效率高、可稳定工作的泵浦调谐范围大等特点，这对于微腔光频率梳的实用化十分重要。但是正常色散区没有类似反常色散区的调制不稳定性效应，需要模式交叉耦合提供局部反常色散来产生四波混频边带或多频率泵浦辅助启动。在正常色散区，Xue等[9]利用单频激光泵浦单个微腔，基于基模和高阶模模式交叉耦合在局部引入反常色散以形成四波混频边带，从而产生光频率梳；Nazemosadat等[10]利用基模和高阶模模式交叉耦合发生模式劈裂来产生光频率梳；Jin等[11]利用光在微环中正反向传播造成模式劈裂产生光频率梳。但是基模和高阶模的交叉耦合模式劈裂点位置难以控制，正反向光耦合产生模式劈裂则需要精确控制相移。此外，也可以采用单频激光泵浦双微环，使得耦合模式发生劈裂，从而产生光频率梳：Xue等[12]利用单频激光泵浦正常色散氮化硅双微环，产生平坦度在10 dB以内的光频率梳；Kim等[13]利用氮化硅双微环结构控制模式交叉耦合的位置以产生光频率梳，将泵浦转换效率提升至41%。上述研究均为单频激光注入微腔并基于四波混频产生频率边带，也可以在微腔中直接输入多频率激光，避免繁杂的调控模式导致交叉耦合或模式劈裂。Weng等[14]利用增益开关调制激光器泵浦微腔，从而产生反常色散光频率梳；Anderson等[15]利用电光调制脉冲泵浦跑道型微腔来产生近零色散Kerr孤子光频率梳。然而，利用多个

收稿日期：2023-09-21；**修回日期**：2023-11-14；**录用日期**：2023-11-21；**网络首发日期**：2023-12-12

基金项目：中央高校基本科研业务费专项资金（2021JBM002）、国家自然科学基金（62275012，62335001）

通信作者：*schfeng@bjtu.edu.cn

电光调制器形成的电光调制脉冲光源体积较大，不利于集成，而锁相双频激光可以看作脉冲光源，可以利用集成分布式反馈（DFB）激光器实现[16]，从而解决电光调制器脉冲泵浦光源体积较大的问题。

氮化硅（Si_3N_4）是目前用于产生光频率梳的主流非线性材料之一，其禁带宽度较大，透明窗口从紫外延伸至红外波段，与标准CMOS工艺兼容；氮化硅材料1550 nm处折射率适中（$n\approx2$），波导尺寸和弯曲半径适中。国外美国哥伦比亚大学、瑞典Chalmers大学、法国CEA-Leti基于减法工艺，瑞士EPFL大学基于倒挖槽Damascene工艺制备的氮化硅波导的损耗已经降到3 dB/m以下[17]；国内南方科技大学刘骏秋、中国科学技术大学董春华等也实现了类似低水平的波导损耗[18-19]，使得基于氮化硅的全集成微腔光频率梳得以实现[20]，从而促进了微腔光频率梳在频率计量、光谱测量、激光雷达测距等方面的应用。通过化学气相沉积法可对氮化硅进行成分调控，形成非线性更强的富硅氮化硅[21]，并且沉积薄膜较厚时不存在应力问题，具有较好的应用前景。目前，基于富硅氮化硅的正常色散区光频率梳的研究还未见报道。因此，本文利用锁相双频激光泵浦正常色散富硅氮化硅微环谐振腔来产生1550 nm波段的光频率梳。通过调节微环谐振腔的几何结构对其色散进行优化设计，通过LLE方程仿真锁相双频激光泵浦微环谐振腔产生光频率梳的腔内时频演变过程，并分析各项参数对光频率梳产生的影响。

2 富硅氮化硅波导色散调控及微环色散

光波导的色散调控优化对于光频率梳的产生具有重要意义，二阶群速度色散（GVD）一般用D来描述，其表达式[22]为

$$D=\frac{\mathrm{d}\tau}{\mathrm{d}\lambda}=-\frac{2\pi c}{\lambda^2}\beta_2\approx-\frac{\lambda}{c}\frac{\mathrm{d}^2 n_{\mathrm{eff}}}{\mathrm{d}\lambda^2},\tag{1}$$

式中：τ为群时延；β_2为二阶群速度色散参量；c为光速；λ为波长；n_{eff}为基模的有效折射率。在模式有效折射率求解仿真中采用Sellmeier公式来计算富硅氮化硅的折射率[23]和SiO_2的折射率[24]。

非线性系数γ的定义为

$$\gamma=\frac{2\pi n_2}{\lambda A_{\mathrm{eff}}},\tag{2}$$

式中：n_2为富硅氮化硅非线性折射率系数[21]；A_{eff}为基模有效模场面积。

利用有限元方法对富硅氮化硅光波导进行模式求解，选择富硅氮化硅多模光波导中TE_0基模进行光频率梳产生的仿真研究，故本实验主要对TE_0基模进行色散调控优化设计。图1(a)展示了富硅氮化硅微环谐振腔的光波导横截面示意图和2200 nm（宽）×600 nm（高）波导能够支持的模式。从图1(c)可以看出，固定波导厚度为600 nm时，富硅氮化硅波导宽度越大，其色散曲线越平稳，色散值β_2整体呈上升趋势；从图1(d)可以看出，固定波导宽度为2200 nm时，随着富硅氮化硅波导厚度增加，色散曲线的极值向长波方向移动，且色散值β_2逐渐降低。为了保证在1550 nm附近获得较为平坦的色散曲线，最终选择富硅氮化硅波导的厚度为600 nm，宽度为2200 nm；同时，计算该波导结构下的有效模场面积A_{eff}和非线性系数γ，如图1(b)所示，在1550 nm处有效模场面积A_{eff}为1.005 μm^2，非线性系数γ为4.587 W^{-1}·m^{-1}。后续将基于该富硅氮化硅波导结构和参数实现光频率梳产生的仿真，并以1550 nm处参数为基准。

此外，需要合理设计1550 nm波段自由光谱范围（FSR；d_{FSR}）为100 GHz的富硅氮化硅微环谐振腔。微环谐振腔的FSR决定所产生的光频率梳相邻梳齿的频率间隔，其对应的表达式（频域，量纲为Hz）为

$$d_{\mathrm{FSR}}=\frac{c}{2\pi R n_{\mathrm{g}}}=\frac{1}{T_{\mathrm{R}}},\tag{3}$$

式中：n_{g}为基模的群折射率，可通过模式有效折射率n_{eff}求得，$n_{\mathrm{g}}=n_{\mathrm{eff}}-\lambda\cdot\partial n_{\mathrm{eff}}/\partial\lambda$；$R$表示圆形微环半径；$T_{\mathrm{R}}$表示光在微环中绕一周需要的时间。

色散会导致微环中不同的谐振纵模模式间的FSR有所变化，即相邻的谐振频率并不是等间距分布的。第μ个纵模的谐振频率ω_μ在中心频率ω_0处的泰勒展开式为

$$\omega_\mu=\omega_0+D_1\mu+\frac{1}{2!}D_2\mu^2+\frac{1}{3!}D_3\mu^3+\cdots,\tag{4}$$

式中：D_k表示k阶色散参数，$D_1=2\pi/(\beta_1 L_{\mathrm{R}})=2\pi d_{\mathrm{FSR}}=2\pi c/(n_{\mathrm{g}}L_{\mathrm{R}})=2\pi/T_{\mathrm{R}}$；$\beta_1$为群时延；$L_{\mathrm{R}}$表示微环的腔长；$D_1/2\pi$表示中心频率处的FSR；$D_2=-\beta_2 D_1{}^2/\beta_1$。为了准确地描述色散对微环的影响，引入色散参量$D_{\mathrm{int}}$，它表示微环中实际的纵模谐振频率与无色散理想情况下的纵模谐振频率之间的偏差量，表达式[25]为

$$D_{\mathrm{int}}=\omega_\mu-(\omega_0+D_1\mu)=\frac{D_2}{2}\mu^2+\frac{D_3}{6}\mu^3+\cdots。\tag{5}$$

考虑波导弯曲对TE_0基模群折射率n_{g}的影响，对微环半径进行迭代优化设计，最终确定微环半径$R=206.5$ μm时，其在1550 nm处的FSR逼近100 GHz，忽略高阶色散，仿真计算其微环色散相关参量、谐振模式间隔$D_1/2\pi$、二阶色散$D_2/2\pi$、三阶色散$D_3/2\pi$、色散参量$D_{\mathrm{int}}/2\pi$。其中$D_1/2\pi=99.95$ GHz，逼近100 GHz，$D_2/2\pi=-4.816$ MHz，$D_3/2\pi=0.008772$ MHz，$D_{\mathrm{int}}/2\pi=-0.005$ GHz，如图2所示。

3 光频率梳产生仿真

正如引言中所述，由于正常色散区没有调制不稳定性效应，若采用单频激光泵浦微腔较难产生光频率梳初始边带。针对这一问题，本文采用锁相双频激光泵浦正常色散富硅氮化硅微环谐振腔来产生光频率

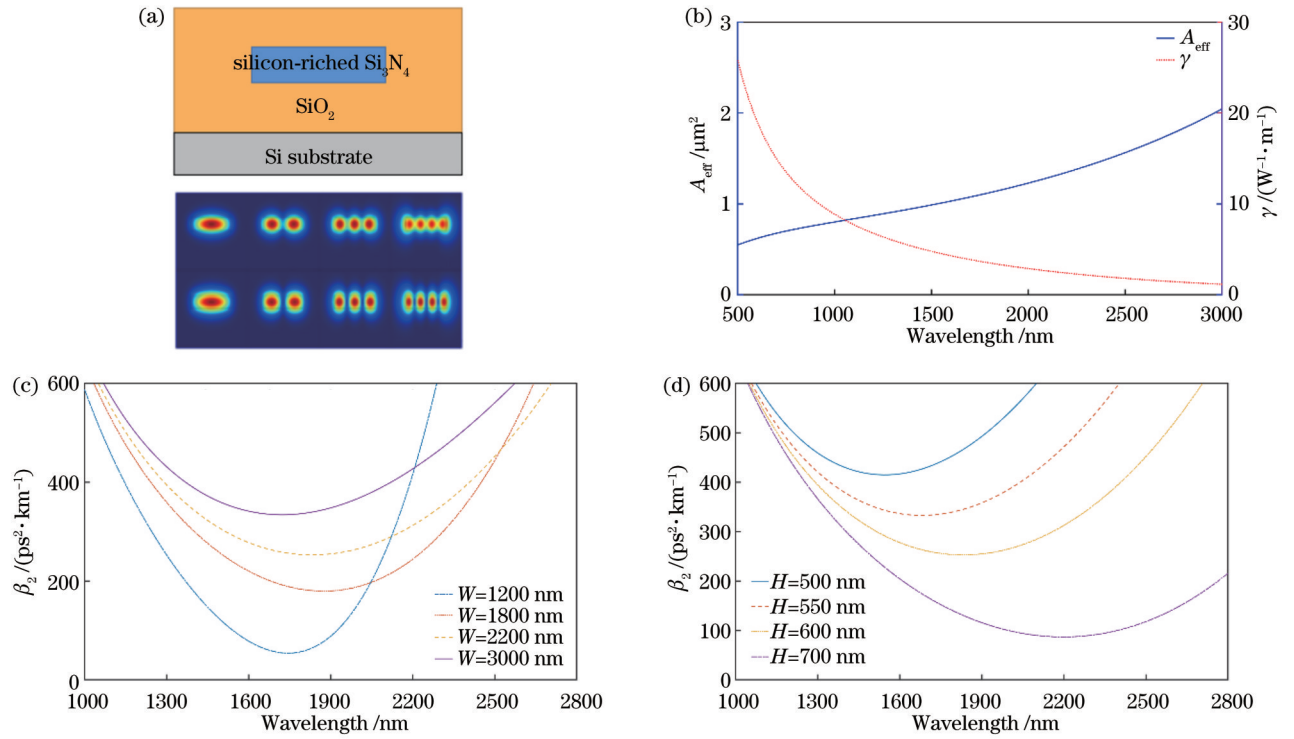

图 1 富硅氮化硅波导色散调控。(a)富硅氮化硅光波导横截面示意图,2200 nm(宽)×600 nm(高)的富硅氮化硅波导支持的模式;(b)最终优化波导中 TE_0 基模有效模场面积 A_{eff} 和非线性系数 γ;(c)高度为 600 nm 时,改变波导宽度的 TE_0 基模色散特性;(d)宽度为 2200 nm 时改变波导高度的 TE_0 基模色散特性

Fig. 1 Dispersion engineering of silicon-riched silicon nitride waveguide. (a) Silicon-riched silicon nitride waveguide cross-section diagram, eigenmodes in the waveguide with 2200 nm width and 600 nm height; (b) A_{eff} and γ of TE_0 mode; (c) simulated TE_0 mode GVD with 600 nm height while change waveguide width; (d) simulated TE_0 mode GVD with 2200 nm width while change waveguide height

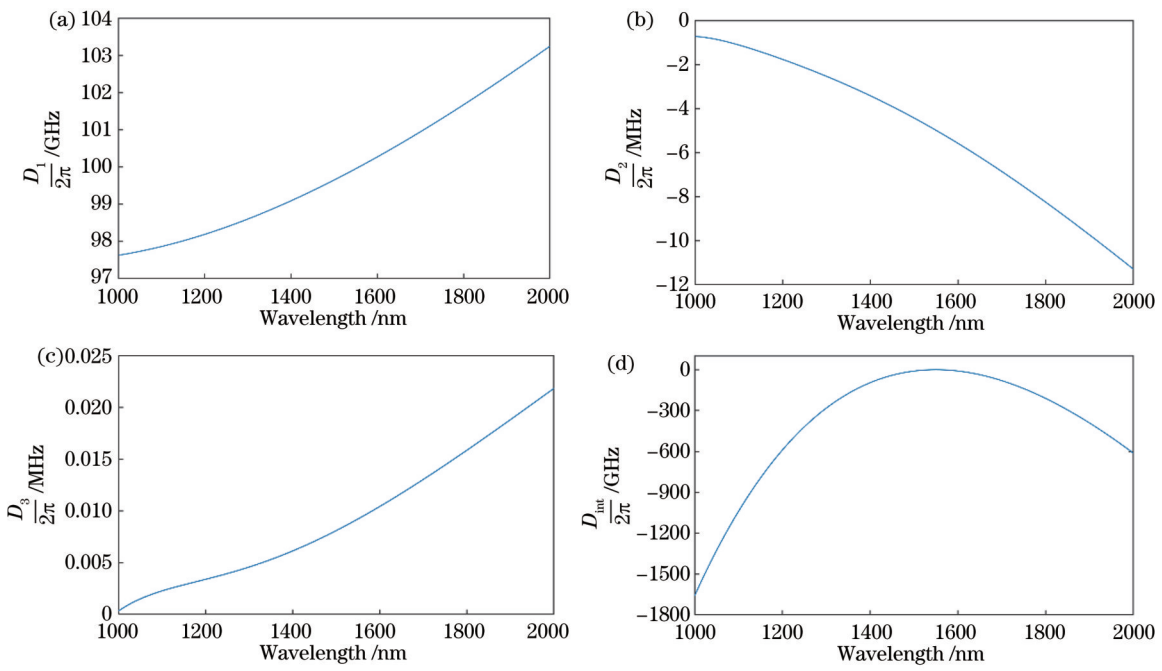

图 2 富硅氮化硅微环色散调控。(a)微环谐振腔谐振模式间隔 $D_1/(2\pi)$;(b)二阶色散 $D_2/(2\pi)$;(c)三阶色散 $D_3/(2\pi)$;(d)色散参量 $D_{int}/(2\pi)$

Fig. 2 Dispersion engineering of silicon-riched silicon nitride microresonator. (a) Resonant mode frequency spacing $D_1/(2\pi)$ of microresonator; (b) second-order dispersion $D_2/(2\pi)$; (c) third-order dispersion $D_3/(2\pi)$; (d) dispersion parameter $D_{int}/(2\pi)$

梳，如图 3 所示。锁相双频激光经掺铒光纤放大器（EDFA）放大后进入富硅氮化硅微环谐振腔，在微环谐振腔中多次传输，随着光场在腔内的能量不断积累，发生级联四波混频并产生更多频率边带，最终稳定输出光频率梳。可以基于欧拉弯曲抑制多模波导中的高阶模式，实现 TE_0 基模高效激发，避免模式交叉耦合影响光频率梳的频谱包络[26]。本文基于 LLE 方程研究微环谐振腔内的光频率梳产生的时频演变过程，由非线性薛定谔方程进一步推导得到 LLE 方程的归一化表达式[27]：

$$\frac{\partial \Psi}{\partial T}=-(1+\mathrm{i}\xi_0)\Psi+\frac{\mathrm{i}}{2}\frac{\partial^2 \Psi}{\partial \varphi^2}+\mathrm{i}|\Psi|^2\Psi+f, \quad (6)$$

式中：归一化变量 $T=t/(2\tau_{ph})$；t 表示光在微环中的总时长；$\tau_{ph}=1/\kappa$ 表示微腔中光子的寿命；$\kappa=\kappa_{ex}+\kappa_0$ 表示微环耦合损耗和波导损耗之和，在光频率梳产生仿真中设定波导损耗和耦合损耗一致，即微环处于临界耦合状态；$\zeta_0=2\delta\omega/\kappa$ 表示泵浦失谐，其中 $\delta\omega$ 表示泵浦激光角频率（本文中指锁相双频激光中一个激光的角频率）和微腔某一谐振峰角频率的差值，可以通过调节泵浦失谐优化光频率梳频谱展宽带宽和平坦度；$\varphi=[\kappa/(2D_2)]^{1/2}\phi$ 表示归一化后的微环方位角，其中 D_2 表示在忽略高阶色散的影响时，实际频率与谐振频率的走离，ϕ 表示微环中光孤子所处微腔的角位置；$\Psi=(2g_0/\kappa)^{1/2}A$ 表示腔内归一化光场，A 表示场的振幅，$g_0=\hbar\omega_0{}^2cn_2/(n_g{}^2V_{eff})$ 表示光子 Kerr 频移，$V_{eff}=A_{eff}L_R$，$f=(P_{in}/P_{threshold})^{1/2}$，$f$ 的值为正数，P_{in} 表示输入的功率，$P_{threshold}=\kappa^3/(8g_0\kappa_{ex})$ 表示产生初级梳齿频率所需的功率。

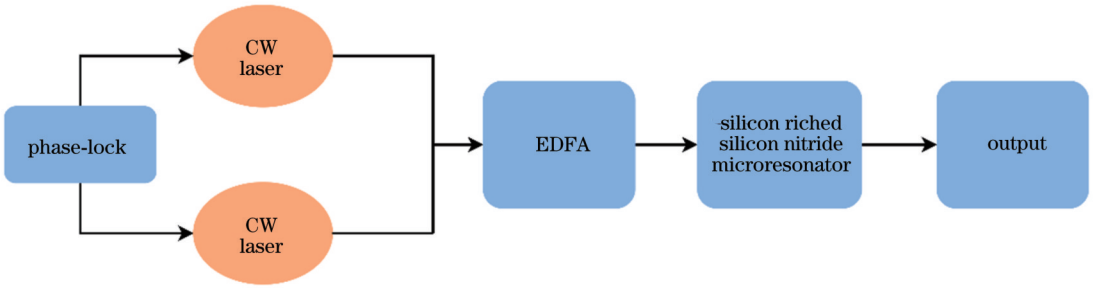

图 3 锁相双频激光泵浦正常色散富硅氮化硅微环谐振腔产生光频率梳示意图

Fig. 3 Schematic of optical frequency comb generation through dual-frequency laser pumping normal dispersion silicon-riched silicon nitride microresonator

相位锁定的双频激光器可看作泵浦激光脉冲源[28]，需要保持双频激光的相对相位恒定，其表达式[29]为

$$A(0,T)=\frac{\sqrt{P_{total}}}{\sqrt{1+x}}\left[1+\sqrt{x}\exp(-2\mathrm{i}\pi v_m T)\right], \quad (7)$$

式中：P_{total} 表示输入的总功率；x 表示高频激光泵浦功率与低频激光泵浦功率的比值；v_m 表示高频激光频率与低频激光频率的差值。

将表 1 中用于光频率梳产生仿真的各项参数代入 LLE 方程，设置锁相双频泵浦激光的频率间隔 v_m 为 100 GHz，微环谐振腔的波导损耗为 40 dB/m，锁相双频激光泵浦的总输入功率为 0.8 W（功率占比为 1），以实际工艺和实验可实现的参数进行光频率梳产生仿真，结果如图 4 所示。根据光频率梳的时频对应关系，可以通过研究单一脉冲的频域光谱包络来分析具有一定重复频率的周期性脉冲光源对应的光频率梳的频域光谱包络。图 4（a）所示为微环谐振腔内平均功率随泵浦失谐的变化曲线，腔内平均功率表示当泵浦失谐为某一数值时腔内各个位置的功率累加取平均。当腔内平均功率最大时，对应的泵浦失谐称为有效零失谐。有效零失谐之前的范围称为有效蓝失谐。在达到有效零失谐后，增大泵浦失谐则腔内平均功率开始降低，故有效零失谐之后的范围称为有效红失谐。在正常色散区通常需要将泵浦失谐调至有效红失谐区才能产生较为平坦的宽带光频率梳。由图 4（a）可知：当泵浦失谐为 12.3 时，腔内平均功率达到最大值，为有效零失谐点；当泵浦失谐为 20.1 时，腔内功率降为 0。本文研究了不同泵浦失谐下的光频率梳的时域和频域特性，图 4（b）为泵浦失谐为 0 时的时域图与频域图，光绕微腔一周的时间为 T_R，故时域脉冲宽度可由其在微腔一周（2π）的脉冲强度占空比等效表示。图 4（c）为泵浦失谐为 6 时的时域和频域图。可以发现，增大泵浦失谐

表 1 仿真产生光频率梳所采用的各项参数

Table 1 Parameters used to simulate the optical frequency comb generation

Parameter	β_2 / ($ps^2 \cdot km^{-1}$)	β_3 / ($ps^3 \cdot km^{-1}$)	β_4 / ($ps^4 \cdot km^{-1}$)	P_0 / W	α / ($dB \cdot m^{-1}$)	$(D_1/2\pi)$ / GHz	$(D_2/2\pi)$ / MHz	$(D_3/2\pi)$ / MHz
Value	284	0.34606	0.001155	0.8	40	100	−4.816	0.00877

时，腔内时域脉冲波形开始变窄，峰值功率增加，频域频谱有所展宽。图 4(d)为泵浦失谐为 12 时的时域和频域图，此时泵浦失谐处于有效零失谐点，腔内时域脉冲峰值功率持续增大，频域初步呈现正常色散光频率梳的典型频谱(两侧“猫耳”)，但平坦度较差。图 4(e)为在有效红失谐区域增大泵浦失谐为 18 时的时域和频域图，其时域脉冲波形持续变窄，峰值功率进一步提高，此时时域光脉冲强度填充率(腔内脉冲占空比)约为 1/4，频谱带宽相比于图 4(d)有明显展宽，平坦度也有一定的提升。图 4(f)为泵浦失谐为 20(有效红失谐区终点附近)时的时域和频域图，其时域脉冲峰值功率虽然相较于图 4(e)提升不明显，但脉冲腔内占空比减小到约 1/6，频域频谱进一步展宽，平坦度得到进一步优化。最终产生了从 1521 nm 到 1583 nm，宽度约 62 nm，平坦度在 10 dB 以内的光频率梳。正常色散微腔中的光频率梳对应的时域脉冲与光纤光学中由非线性薛定谔方程得到的暗孤子有所不同，研究者们通常称之为“暗脉冲”(dark pulse)或者“平顶脉冲”(platicon)，而暗脉冲和平顶脉冲在本质上没有区别，仅是描述微腔一个周期内脉冲的高功率和低功率部分相对占空比不同时的情况[30]。在正常色散区产生光频率梳的过程中，微腔腔内光功率不会发生大的突变，因此微腔谐振峰不会因为腔内热效应而发生大的漂移，可以避免快速扫频等技术的使用，实验上更加容易实现，即正常色散微腔产生光频率梳有较大的泵浦失谐可调节范围，有利于光频率梳的实际产生。但是调节泵浦失谐，会改变光频率梳频谱宽度及相对应的微腔内的脉冲宽度。由以上的分析可知，如果要确保光频率梳的稳定运转(腔内脉冲宽度及光谱形状稳定不变)，需要产生光频率梳时保持一定的泵浦失谐。

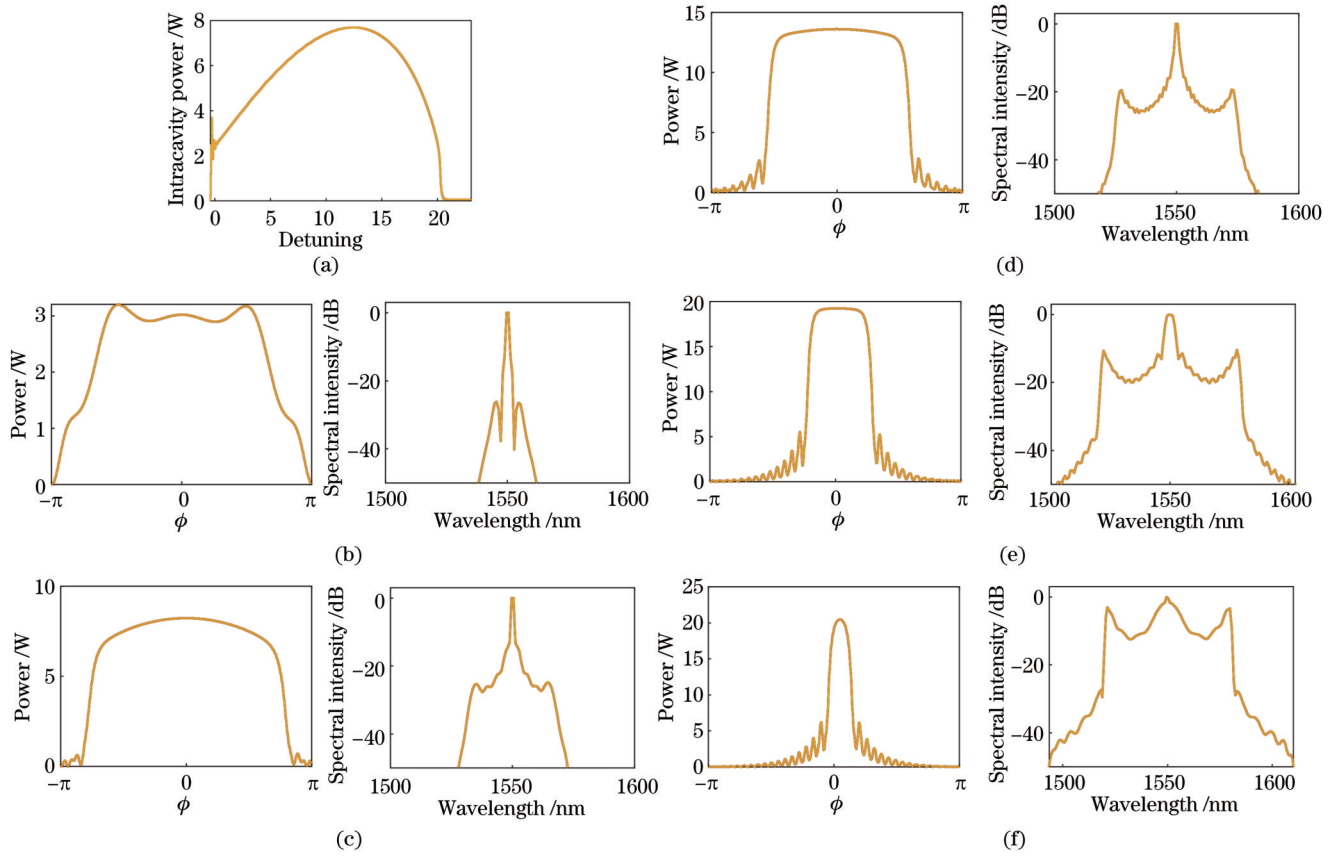

图 4 锁相双频激光泵浦正常色散富硅氮化硅微环谐振腔仿真产生光频率梳的时频演化。(a)腔内平均功率随着泵浦失谐的演化；(b)泵浦失谐为 0 时腔内时域脉冲和对应频谱的演化；(c)泵浦失谐为 6 时腔内时域脉冲和对应频谱的演化；(d)泵浦失谐为 12 时腔内时域脉冲和对应频谱的演化；(e)泵浦失谐为 18 时腔内时域脉冲和对应频谱的演化；(f)泵浦失谐为 20 时腔内时域脉冲和对应频谱的演化

Fig. 4 Time-frequency evolution process of optical frequency comb generation in normal dispersion silicon-riched silicon nitride microresonator pumped by phase-locked dual-frequency laser. (a) Average intracavity power evolution with pump detuning; (b) evolution of time domain pulse and corresponding spectrum when pump detuning is 0; (c) evolution of time domain pulse and corresponding spectrum when pump detuning is 6; (d) evolution of time domain pulse and corresponding spectrum when pump detuning is 12; (e) evolution of time domain pulse and corresponding spectrum when pump detuning is 18; (f) evolution of time domain pulse and corresponding spectrum when pump detuning is 20

基于正常色散微环谐振腔产生光频率梳受到众多参数的影响，本文研究了几种不同参量对光频率梳产生的影响。首先，研究锁相双频激光泵浦功率对光频率梳产生的影响。保持上述仿真中其他条件不变，将锁相双频激光的泵浦功率设置为0.1、0.4、0.8 W，研究腔内光频率梳的时频演变情况。图5(a)给出了不同泵浦功率下腔内平均功率随着泵浦失谐的变化曲线。可以看到，随着泵浦功率的减小，腔内平均功率减小，有效零失谐点左移，有效红失谐区(即可产生较平坦光频率梳对应的泵浦失谐区)减小。图5(b)给出了不同泵浦功率下的腔内时域脉冲波形，在相同的时域脉冲强度填充率(即脉冲占空比)下，泵浦功率的减小明显降低了腔内时域脉冲的峰值功率。图5(c)给出了不同泵浦功率下时域脉冲强度填充率相同时对应光频率梳的频谱。当泵浦功率减小到0.4 W时，光频率梳的频谱带宽减小，但平坦度没有受到太大影响；当泵浦功率减小到0.1 W时，光频率梳的平坦度有所降低，同时光频率梳频谱带宽减小。由以上分析可知，增大泵浦功率，则增大了微腔内的光功率强度，等效于提高了腔内的非线性，在时域脉冲强度填充率相同时，可以获得较大的光频率梳频谱带宽。另外，若增大基模的非线性系数γ，也可以获得较大的光频率梳频谱带宽[31]。

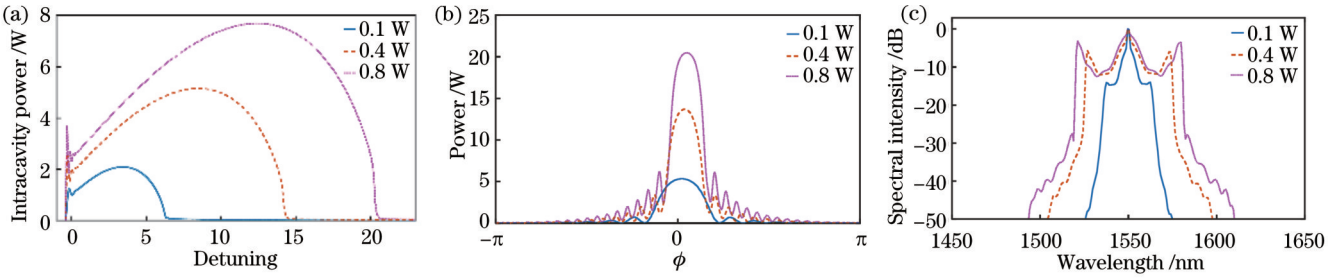

图5 输入泵浦功率对光频率梳产生的影响。(a)不同泵浦功率下随泵浦失谐的腔内平均功率演化；(b)不同泵浦功率下在时域脉冲强度填充率相同时的时域脉冲；(c)不同泵浦功率下在时域脉冲强度填充率相同时的光频率梳频谱图

Fig. 5 Influence of input pump power on optical frequency comb generation. (a) Evolution of average intracavity power with pump detuning under different pump powers; (b) time-domain pulses with different pump powers when pulse intensity filling rate is same; (c) optical frequency comb spectra with different pump powers at the same pulse intensity filling rate

其次，研究不同锁相双频激光功率占比x对光频率梳产生的影响。保持上述仿真中其他条件不变，将锁相双频激光功率占比分别设置为0.5、1.0、1.5，研究腔内光频率梳的时频演变情况。图6(a)给出了锁相双频激光功率占比x不同时腔内平均功率随着泵浦失谐的变化曲线。可以看到，双频激光功率占比x的变化对泵浦失谐的可调谐范围影响较小。图6(b)、(c)分别给出了双频激光功率占比x不同时，相同时域脉冲强度填充率下的腔内时域脉冲波形及对应的光频率梳频谱。可以看到，改变锁相双频激光功率占比x，对腔内时域脉冲波形峰值功率及光频率梳频谱几乎没有影响。

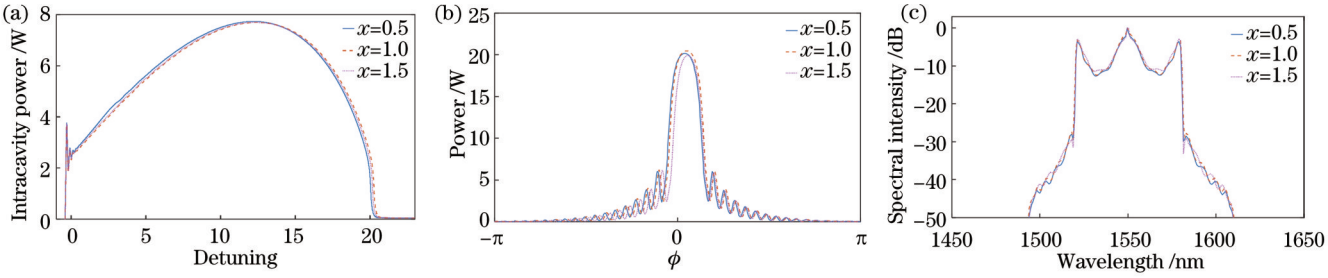

图6 双频激光功率占比对光频率梳产生的影响。(a)不同双频激光功率占比下随泵浦失谐的腔内平均功率演化；(b) 不同功率占比下在时域脉冲强度填充率相同时的时域脉冲；(c) 不同功率占比下在时域脉冲强度填充率相同时光频率梳频谱

Fig. 6 Influence of dual-frequency laser power ratio on optical frequency comb generation. (a) Evolution of average intracavity power with pump detuning under different dual-frequency laser power ratios; (b) time-domain pulses with different laser power ratios when the pulse intensity filling rate is same; (c) optical frequency comb spectra with different laser power ratios at the same pulse intensity filling rate

再次，研究微环波导损耗对光频率梳产生的影响。保持上述仿真中其他条件不变，将波导损耗分别设置为20 dB/m、40 dB/m和60 dB/m，研究腔内光频率梳的时频演变情况。图7(a)给出了不同微环波导损耗下腔内平均功率随着泵浦失谐的变化曲线。可以看到，波导损耗增大使得腔内平均功率降低，有效零失谐点左移，有效红失谐区域缩小，与降低双频激光泵浦功率的影响类似。图7(b)给出了不同波导损耗下腔内

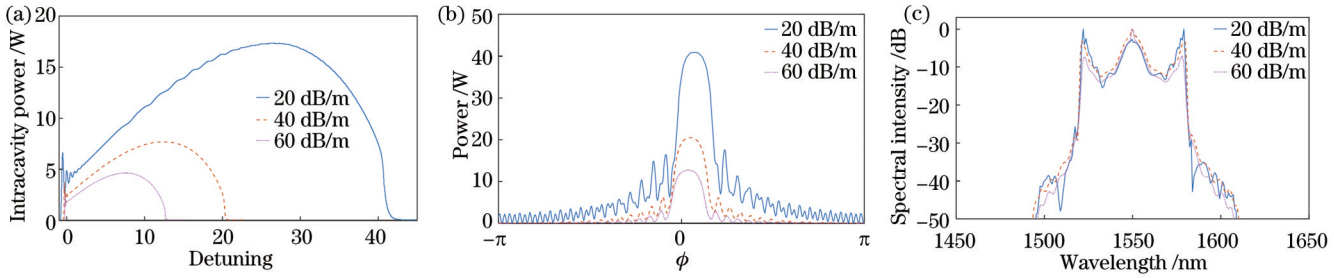

图 7 微环波导损耗对光频率梳产生的影响。(a)不同损耗下随泵浦失谐的腔内平均功率演化;(b)不同损耗下在时域脉冲强度填充率相同时的时域脉冲;(c)不同损耗下在时域脉冲强度填充率相同时的光频率梳频谱

Fig. 7 Influence of waveguide loss on optical frequency comb generation. (a) Evolution of average intracavity power with pump detuning under different waveguide losses; (b) time-domain pulses with different waveguide losses when the pulse intensity filling rate is same; (c) optical frequency comb spectra with different waveguide losses at the same pulse intensity filling rate

光频率梳的时域波形,在相同时域脉冲强度填充率下,波导损耗的增大使得腔内时域脉冲的峰值功率明显降低,这也类似于降低双频激光泵浦功率的影响。图 7(c)给出了不同波导损耗下时域脉冲强度填充率相同时腔内产生光频率梳的频谱图,其频谱范围基本相同。

然后,研究微环色散对光频率梳产生的影响。上述仿真中微环谐振腔的微环色散 $D_2/(2\pi)=-4.816$ MHz,对应的 β_2 为 284 ps^2/km。保持上述仿真中其他条件不变,选取前述色散调控中一些其他正常色散值进行光频率梳产生仿真并进行对比。用于对照的其他两组波导分别为:截面高 650 nm、宽 1800 nm 的微环色散 $D_2/(2\pi)=-3.510$ MHz(对应的 β_2 为 198 ps^2/km),以及截面高 450 nm、宽 3000 nm 的微环色散 $D_2/(2\pi)=-9.631$ MHz(对应的 β_2 为 566 ps^2/km),二者的微环半径均为 206.5 μm。图 8(a)给出了不同色散下的腔内平均功率随泵浦失谐变化的曲线。可以看到,色散绝对值增大基本不会影响有效零失谐点的位置,在有效蓝失谐区,不同色散的腔内平均功率变化曲线基本重合。色散绝对值的增大使得有效红失谐区的终点位置左移,即产生光频率梳的泵浦失谐区间减小。图 8(b)给出了不同色散情况下腔内光频率梳的时域脉冲波形,在相同时域脉冲强度填充率下,色散绝对值的增加使得腔内脉冲峰值功率略有降低。图 8(c)给出了不同色散情况下腔内产生光频率梳的频谱图,可以看到,在相同时域脉冲强度填充率下,色散绝对值的增加使得光频率梳的频谱带宽明显减小,而平坦度基本不受影响。

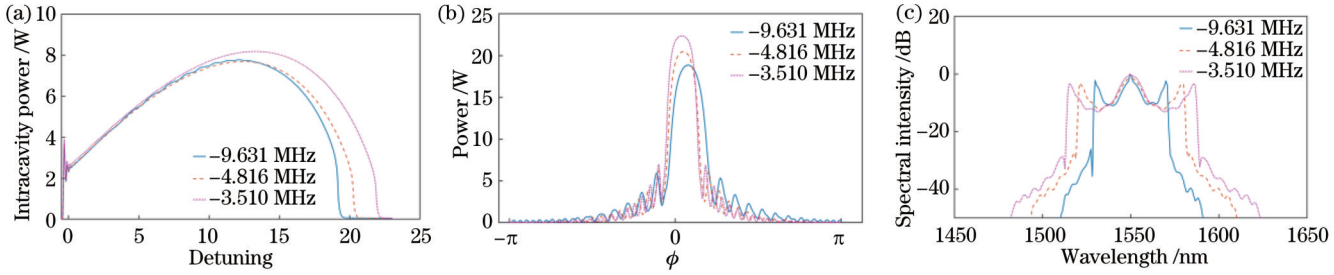

图 8 微环色散对光频率梳产生的影响。(a)不同色散下随泵浦失谐的腔内平均功率演化;(b)不同色散下在时域脉冲强度填充率相同时的时域脉冲;(c)不同色散下在时域脉冲强度填充率相同时的光频率梳频谱

Fig. 8 Influence of microresonator dispersion on optical frequency comb generation. (a) Evolution of average intracavity power with pump detuning under different dispersions; (b) time-domain pulses with different dispersions when pulse intensity filling rate is same; (c) optical frequency comb spectra with different dispersions at the same pulse intensity filling rate

最后,研究锁相双频激光频率间隔对光频率梳产生的影响。保持上述仿真中的其他条件不变,将双频激光频率间隔分别设置为 100、200、300 GHz,研究腔内光频率梳的时频演变情况。图 9(a)给出了输入双频激光的频率间隔不同时腔内平均功率随着泵浦失谐的变化曲线。可以看到,双频激光频率间隔增大使得腔内平均功率略有升高,双频激光频率间隔为 1 倍 FSR 时,其泵浦失谐的可调谐范围最大。从图 9(b)可以看到,在相同时域脉冲强度填充率下,不同的双频激光频率间隔对应腔内有不同个数的脉冲,即:双频激光频率间隔为 1 倍 FSR 时,对应腔内出现 1 个脉冲;双频激光频率间隔为 2 倍 FSR 时,对应腔内出现 2 个脉冲;双频激光频率间隔为 3 倍 FSR 时,对应腔内出现 3 个脉冲。图 9(c)~(e)给出了在相同时域脉冲强度填充率下 3 种不同双频激光频率间隔对应的频谱图,梳齿间隔与双频激光频率间隔一致,双频激光频率间隔为

多倍FSR时，部分单倍FSR梳齿仍被激发（但功率较低），该现象原因有待进一步研究。

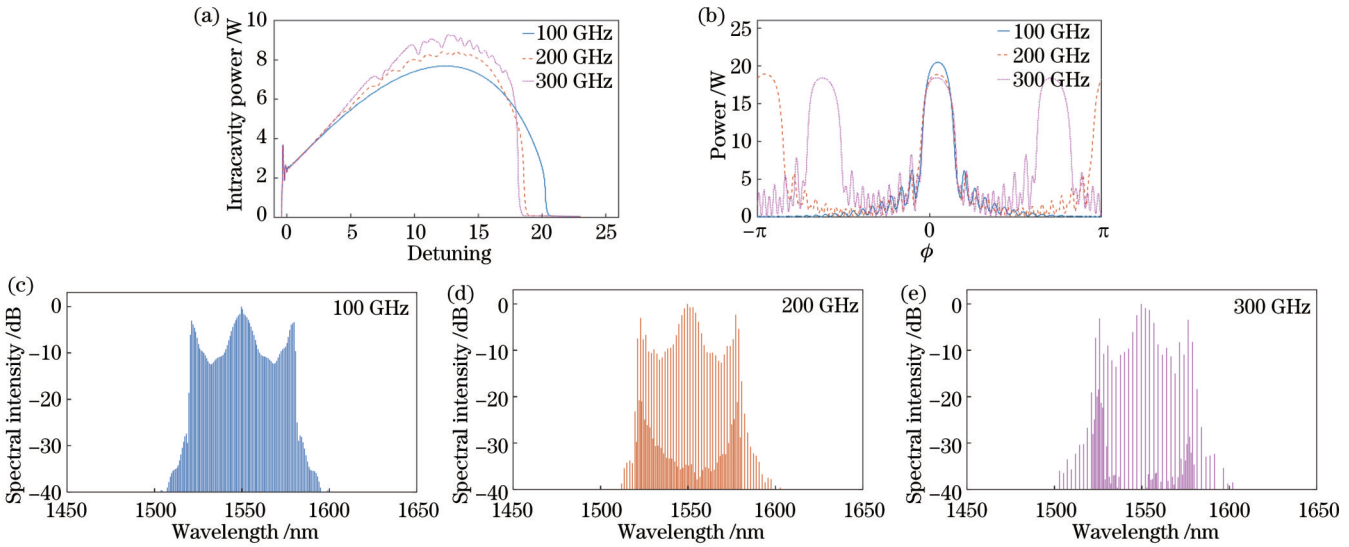

图9　双频激光频率间隔对光频率梳产生的影响。(a)不同频率间隔下腔内平均功率随泵浦失谐的演化；(b) 不同频率间隔下时域脉冲强度填充率相同时的时域脉冲；双频激光频率间隔为(c)一倍FSR、(d)二倍FSR、(e)三倍FSR的频谱

Fig. 9　Influence of dual-frequency laser frequency interval on optical frequency comb generation. (a) Evolution of average intacavity power with pump detuning under different frequency intervals; (b) time domain pulses with different frequency intervals when pulse intensity filling rate is same; optical frequency comb spectra with (c) one, (d) two, and (e) three FSR frequency intervals at the same pulse intensity filling rate

4　结　　论

对基于锁相双频激光泵浦正常色散富硅氮化硅微环谐振腔在1550 nm波段产生光频率梳进行仿真研究。对富硅氮化硅微环谐振腔多模光波导的TE_0基模进行色散调控和优化设计，实现了1550 nm波段平坦正常色散。利用LLE方程进行光频率梳产生仿真，分析泵浦失谐改变时腔内光频率梳产生的时域和频域演化过程。同时，探究锁相双频激光泵浦功率、锁相双频激光功率占比x、微腔波导损耗、微腔色散、双频激光频率间隔等参数对光频率梳产生的影响。仿真实现的光频率梳带宽可覆盖1520 nm到1580 nm。从仿真结果中得出，锁相双频泵浦正常色散微环谐振腔产生光频率梳有较大的泵浦可调谐范围，有利于光频率梳的实际产生和长期稳定工作。本文结果有助于推动基于正常色散富硅氮化硅微环谐振腔产生1550 nm波段宽带集成光频率梳的研究和应用。

参　考　文　献

[1] Bartels A, Heinecke D, Diddams S A. Passively mode-locked 10 GHz femtosecond Ti: sapphire laser[J]. Optics Letters, 2008, 33(16): 1905-1907.

[2] Duan G H, Shen A, Akrout A, et al. High performance InP-based quantum dash semiconductor mode-locked lasers for optical communications[J]. Bell Labs Technical Journal, 2009, 14(3): 63-84.

[3] 赵欣，杨建军，张力钎，等. 单腔双光梳技术[J]. 中国激光，2022，49(19)：1901003.
Zhao X, Yang J J, Zhang L Q, et al. Single-cavity dual-comb technology[J]. Chinese Journal of Lasers, 2022, 49(19): 1901003.

[4] Beha K, Cole D C, Del'Haye P, et al. Electronic synthesis of light[J]. Optica, 2017, 4(4): 406-411.

[5] Hu H, Da Ros F, Pu M H, et al. Single-source chip-based frequency comb enabling extreme parallel data transmission[J]. Nature Photonics, 2018, 12(8): 469-473.

[6] Kippenberg T J, Gaeta A L, Lipson M, et al. Dissipative Kerr solitons in optical microresonators[J]. Science, 2018, 361(6402): eaan8083.

[7] 匡全进，谢成峰，王梦宇，等. 研究基于超高Q值氟化钙晶体微腔的非线性散射效应研究[J]. 光学学报，2023，43(16)：1623021.
Kuang Q J, Xie C F, Wang M Y, et al. Nonlinear scattering effect based on ultrahigh-Q factor CaF_2 crystal microcavity[J]. Acta Optica Sinica, 2023, 43(16): 1623021.

[8] 戴键，李鑫敏，刘安妮，等. 基于氟化镁微腔孤子光频梳的低相噪微波信号产生[J]. 光学学报，2022，42(20)：2007001.
Dai J, Li X M, Liu A N, et al. Low phase noise microwave signal generation based on soliton frequency comb in MgF_2 microresonator[J]. Acta Optica Sinica, 2022, 42(20): 2007001.

[9] Xue X X, Xuan Y, Liu Y, et al. Mode-locked dark pulse Kerr combs in normal-dispersion microresonators[J]. Nature Photonics, 2015, 9(9): 594-600.

[10] Nazemosadat E, Fülöp A, Helgason Ó B, et al. Switching dynamics of dark-pulse Kerr frequency comb states in optical microresonators[J]. Physical Review A, 2021, 103: 013513.

[11] Jin W, Yang Q F, Chang L, et al. Hertz-linewidth semiconductor lasers using CMOS-ready ultra-high-Q microresonators[J]. Nature Photonics, 2021, 15(5): 346-353.

[12] Xue X X, Xuan Y, Wang P H, et al. Normal-dispersion microcombs enabled by controllable mode interactions[J]. Laser & Photonics Reviews, 2015, 9(4): L23-L28.

[13] Kim B Y, Okawachi Y, Jang J K, et al. Turn-key, high-efficiency Kerr comb source[J]. Optics Letters, 2019, 44(18): 4475-4478.

[14] Weng W L, Kaszubowska-Anandarajah A, He J J, et al. Gain-switched semiconductor laser driven soliton microcombs[J]. Nature Communications, 2021, 12: 1425.
[15] Anderson M H, Weng W L, Lihachev G, et al. Zero dispersion Kerr solitons in optical microresonators[J]. Nature Communications, 2022, 13: 4764.
[16] Rahim M, Zeb K, Lu Z G, et al. Monolithic InAs/InP quantum dash dual-wavelength DFB laser with ultra-low noise common cavity modes for millimeter-wave applications[J]. Optics Express, 2019, 27(24): 35368-35375.
[17] Sun Z Y, Li Y, Bai B F, et al. Silicon nitride-based Kerr frequency combs and applications in metrology[J]. Advanced Photonics, 2022, 4(6): 064001.
[18] Ye Z C, Jia H Y, Huang Z J, et al. Foundry manufacturing of tight-confinement, dispersion-engineered, ultralow-loss silicon nitride photonic integrated circuits[J]. Photonics Research, 2023, 11(4): 558-568.
[19] Wan S, Niu R, Peng J L, et al. Fabrication of the high-Q Si_3N_4 microresonators for soliton microcombs[J]. Chinese Optics Letters, 2022, 20(3): 032201.
[20] Xiang C, Liu J Q, Guo J, et al. Laser soliton microcombs heterogeneously integrated on silicon[J]. Science, 2021, 373(6550): 99-103.
[21] Ye Z C, Fülöp A, Helgason Ó B, et al. Low-loss high-Q silicon-rich silicon nitride microresonators for Kerr nonlinear optics[J]. Optics Letters, 2019, 44(13): 3326-3329.
[22] 刘宇, 邓宜, 卫航, 等. 基于薄膜铌酸锂光波导的平坦光频率梳的设计[J]. 中国激光, 2021, 48(13): 1301001.
Liu Y, Deng Y, Wei H, et al. Design of flat optical frequency comb based on lithium niobate optical waveguide[J]. Chinese Journal of Lasers, 2021, 48(13): 1301001.
[23] Wu C L, Lin Y H, Su S P, et al. Degenerate four-wave mixing in Si quantum dot doped Si-rich SiN_x channel waveguide[J]. Journal of Lightwave Technology, 2016, 34(17): 4111-4120.
[24] Malitson I H. Interspecimen comparison of the refractive index of fused silica[J]. Journal of the Optical Society of America, 1965, 55(10): 1205-1208.
[25] Herr T, Brasch V, Jost J D, et al. Temporal solitons in optical microresonators[J]. Nature Photonics, 2014, 8(2): 145-152.
[26] 邓宜. 基于脉冲同步泵浦正常色散微环谐振腔的光频率梳研究[D]. 北京: 北京交通大学, 2022.
Deng Y. Study on optical frequency comb based on pulse synchronous pumping normal dispersion microring resonator[D]. Beijing: Beijing Jiaotong University, 2022.
[27] Chembo Y K, Menyuk C R. Spatiotemporal Lugiato-Lefever formalism for Kerr-comb generation in whispering-gallery-mode resonators[J]. Physical Review A, 2013, 87(5): 053852.
[28] Tong Z, Wiberg A O J, Myslivets E, et al. Spectral linewidth preservation in parametric frequency combs seeded by dual pumps[J]. Optics Express, 2012, 20(16): 17610-17619.
[29] Antikainen A, Agrawal G P. Dual-pump frequency comb generation in normally dispersive optical fibers[J]. Journal of the Optical Society of America B, 2015, 32(8): 1705-1711.
[30] Wang W Q, Wang L R, Zhang W F. Advances in soliton microcomb generation[J]. Advanced Photonics, 2020, 2(3): 034001.
[31] Guo B, Guo X Y, Tang L G, et al. Ultra-long-period grating-based multi-wavelength ultrafast fiber laser[J]. Chinese Optics Letters, 2021, 19(7): 071405.

Design of Optical Frequency Comb Based on Dual-Frequency Pumped Normal Dispersion Silicon-Riched Silicon Nitride Microresonator

Yang Yanan[1], Gao Rong[1], Zhan Chenyi[1], Li Ding[1], Deng Yi[1], Wang Zixiao[1], Liang Kun[2], Feng Suchun[1*]

[1]*Key Laboratory of All Optical Network and Advanced Telecommunication Network, Ministry of Education, Institute of Lightwave Technology, School of Electronic and Information Engineering, Beijing Jiaotong University, Beijing* 100044, *China*;

[2]*School of Electronic and Information Engineering, Beijing Jiaotong University, Beijing* 100044, *China*

Abstract

Objective Generation schemes of optical frequency combs mainly include mode-locked laser, electro-optic modulation comb, nonlinear supercontinuum-based comb, and nonlinear Kerr microresonator comb. Compared with other generation methods of optical frequency combs, the Kerr microresonator comb is considered a new type of coherent light source that features unique and promising advantages of lower power consumption and whole system integratability.

The Kerr microresonator pumped in the anomalous group velocity dispersion (GVD) regime leads to the dissipative Kerr soliton comb. The dissipative soliton states are sometimes inaccessible due to the intracavity thermal dynamics and therefore require special tricks to align the pump laser and the resonances in soliton formation. These approaches need benchtop laser sources and complex control protocols, which are not suitable for integrated photonic systems. Furthermore, due to the small temporal overlap between the driving continuum wave laser and the ultrashort pulse, the pump-to-comb conversion efficiency is rather low. Meanwhile, Kerr comb pumped in the normal GVD regime has the benefits including relatively easy access to high pump-to-comb conversion efficiency, large pump frequency detuning range for comb generation, and lower power falloffs within the spectral region of interest which are more ideal for optical communications. Since there is no modulation instability (MI) in the normal GVD regime, the most prevalent method to

generate a normal GVD comb is to modify the microresonator dispersion via mode splitting. Common mode splitting mechanisms contain mode coupling to different polarization modes, spatial modes, injection locking, and auxiliary resonator modes. However, the above-mentioned methods are quite complicated. Another method to generate a normal GVD comb can be achieved by pump direct modulation or electro-optic pulse generator based on electro-optic intensity and phase modulators at the resonator free spectral range (FSR), but the electro-optic pulse generator is quite bulky. The phase-locked dual-frequency laser can be regarded as a pulse pump laser source with a wide pulse duration, which can be realized by an integrated DFB laser.

Silicon nitride is widely applied to nonlinear optics. It has an ultra-broad transparency window, low intrinsic loss, and a refractive index that allows for moderate optical field confinement in waveguides. However, fabricating thick films with high yield is challenging owing to the large tensile stress in as-deposited stoichiometric silicon nitride films, which can result in the formation of cracks crossing the photonic devices. An alternative way to overcome the high tensile stress is varying the composition of the material itself. In particular, silicon-riched silicon nitride can dramatically reduce the film stress. Silicon-riched silicon nitride waveguides also have a higher nonlinear Kerr coefficient and refractive index than stoichiometric silicon nitride, but the normal GVD comb based on the silicon-riched silicon nitride has not been reported. Thus, we propose a generation scheme of optical frequency combs by adopting a phase-locked dual-frequency laser-pumped normal dispersion silicon-riched silicon nitride microresonator. The proposed optical frequency comb has potential applications in astronomy, optical communication, and microwave photonics.

Methods Firstly, the flat normal dispersion in the 1550 nm band is realized via dispersion engineering of the silicon-riched silicon nitride microresonator by the finite element method mode solver. The effective mode field area of the TE_0 fundamental mode at 1550 nm in the optimized silicon-riched silicon nitride waveguide is about 1.005 μm^2, and the nonlinear coefficient is about 4.587 $W^{-1}\cdot m^{-1}$. Meanwhile, the dispersion parameters of the microresonator with 100 GHz free spectral range (FSR) are also optimized. Then, the optical frequency comb generation pumped by a phase-locked dual-frequency laser based on the normal dispersion silicon-riched silicon nitride microresonator is simulated by employing the Lugiato Lefever equation (LLE). The evolution process of the optical frequency comb in time and frequency domains related to the laser pump detuning is studied. Additionally, the effects of several parameters on the performance of the optical frequency comb are also investigated.

Results and Discussions The silicon-riched silicon nitride waveguide structure with optimized normal dispersion and nonlinear coefficient is obtained by dispersion engineering (Fig. 1). The dispersion parameters such as resonant mode frequency spacing $D_1/(2\pi)$, second-order dispersion $D_2/(2\pi)$, third-order dispersion $D_3/(2\pi)$, dispersion parameter $D_{int}/(2\pi)$ of a microresonator with bending radius of 206.5 μm are also obtained (Fig. 2). The schematic diagram of the optical frequency comb generated via phase-locked dual-frequency laser pumped normal dispersion silicon-riched silicon nitride microresonator is shown (Fig. 3). The optical frequency comb generation is simulated by the LLE. The time-frequency evolution process of the optical frequency comb in time and frequency domains related to the pump detuning is studied (Fig. 4). The optical frequency comb in the normal GVD regime can be generated within a relatively large pump detuning range. The laser pump detuning is intrinsically linked to the intensity filling rate of a pulse state. When the pump detuning increases, the pulse becomes narrow with a broad corresponding spectrum. The effects of several parameters such as the pump power, the power proportion of the dual-frequency laser, microresonator waveguide loss, microresonator dispersion, and the frequency interval of dual-frequency laser on the performance of the optical frequency comb are also investigated. The following conclusions can be obtained by the simulation. Firstly, under the higher laser pump power, the pump detuning range for the optical frequency comb generation becomes larger and the pulse peak power under the same pulse intensity filling rate increases, with a wider corresponding spectrum (Fig. 5). Secondly, the power proportion of dual-frequency laser has little influence on optical frequency comb generation (Fig. 6). Thirdly, when the microresonator waveguide loss is larger, the pump detuning range for optical frequency comb generation becomes smaller, and the pulse peak power under the same pulse intensity filling rate decreases (Fig. 7). Fourthly, with the increasing absolute dispersion value, the spectrum bandwidth of the optical frequency comb under the same pulse intensity filling rate reduces obviously (Fig. 8). Finally, the frequency spacing of the optical frequency comb can be tuned via changing the frequency spacing of the phase-locked dual-frequency laser with integral multiple of FSR (Fig. 9).

Conclusions We propose a generation scheme of optical frequency combs by adopting a phase-locked dual-frequency laser-pumped normal dispersion silicon-riched silicon nitride microresonator. By optimizing the structure of silicon-riched silicon nitride microresonator and dispersion engineering, an optical frequency comb with bandwidth from 1520 nm to 1580 nm is realized via the simulation. The time-frequency evolution process of optical frequency comb generation is analyzed. The simulation results show that a dual-frequency pumped optical frequency comb in the normal GVD regime

can be generated within a relatively large pump detuning range, which will benefit long-term comb stabilization and real applications. Additionally, the effects on the performance of optical frequency combs such as the pump power, the power proportion of the dual-frequency laser, microresonator waveguide loss, microresonator dispersion, and the frequency interval of dual-frequency lasers are also studied. Our study shows that silicon-riched silicon nitride waveguides have potential benefits for the 1550 nm broadband optical frequency comb based on normal dispersion nonlinear optical microresonator.

Key words nonlinear optics; optical frequency comb; silicon-riched silicon nitride; dispersion engineering; microresonator